Direct Determination of the Chemical Bonding of Individual Impurities in Graphene

Wu Zhou,[1,2,*] Myron D. Kapetanakis,[1,2] Micah P. Prange,[1,2,†] Sokrates T. Pantelides,[1,2] Stephen J. Pennycook,[2,1] and Juan-Carlos Idrobo[2,*]

[1]*Department of Physics and Astronomy, Vanderbilt University, Nashville, Tennessee 37235, USA*

[2]*Materials Science and Technology Division, Oak Ridge National Laboratory, Oak Ridge, Tennessee 37831, USA*

(Received 19 September 2012; published 15 November 2012)

Using a combination of *Z*-contrast imaging and atomically resolved electron energy-loss spectroscopy on a scanning transmission electron microscope, we show that the chemical bonding of individual impurity atoms can be deduced experimentally. We find that when a Si atom is bonded with four atoms at a double-vacancy site in graphene, Si 3*d* orbitals contribute significantly to the bonding, resulting in a planar sp^2d-like hybridization, whereas threefold coordinated Si in graphene adopts the preferred sp^3 hybridization. The conclusions are confirmed by first-principles calculations and demonstrate that chemical bonding of two-dimensional materials can now be explored at the single impurity level.

DOI: 10.1103/PhysRevLett.109.206803 PACS numbers: 73.22.Pr, 68.37.Ma, 71.55.−i, 79.20.Uv

Unveiling the local structure and bonding characteristics at the atomic scale is a goal in many analytical techniques. Scanning tunneling microscopy is capable of providing information about the local structure and surface density of states at the atomic scale [1,2]. Similarly, high-resolution transmission electron microscopy (TEM) imaging, supplemented by density functional theory (DFT) calculations, can provide evidence of charge redistribution in two-dimensional materials at the single-atom level [3]. However, direct determination of the chemical identities and bonding characteristics of individual atoms has not been achieved with these two techniques. On the other hand, simultaneous annular dark-field (ADF) imaging and electron energy loss spectroscopy (EELS) [4–10] on an aberration-corrected scanning transmission electron microscope (STEM) has been demonstrated to be a powerful method for atom-by-atom structural and elemental identification. Moreover, the energy-loss near-edge fine structure (ELNES) [5] available in EELS can also provide rich information about the bonding and local electronic structure of the element studied. Recently, using ELNES, different electronic structure features of carbon atoms at a graphene edge were revealed [10].

Obtaining the bonding information via ELNES from individual impurity or dopant atoms in the material, and correlating the bonding with local atomic configurations, however, is still a challenge due to the extremely weak signal and limited sample stability under the electron beam irradiation. Here, we overcome these difficulties and demonstrate direct determination and differentiation of sp^3 and sp^2d-like hybridization of different configurations of Si impurities in graphene using a combination of ADF imaging and atomically resolved EELS on an aberration-corrected STEM (see Supplementa Material for details [11]).

Si is one of the most common impurities in graphene grown by chemical vapor deposition [12,13], due to the presence of Si sources (Si/SiO_2 wafer, quartz tube, *etc*) during the high-temperature growth process and the isovalence of Si and C. Si impurities are also expected to be intrinsically present in epitaxial graphene obtained via thermal decomposition of SiC [14,15], and could have significant influence on the transport properties of graphene samples [2,16,17]. Therefore, a better understanding of the local electronic structure and the nature of the chemical bonding of individual Si impurities in the graphene lattice is desirable, especially for the integration of graphene-based nanodevices onto the silicon platform [18,19].

The atomic configuration of Si impurities in graphene was studied using ADF imaging on an aberration-corrected STEM operating at 60 kV, which is below the knock-on damage threshold of graphene. Figure 1 shows typical STEM-ADF images and corresponding structure models for several stable Si point defects in graphene. The Si atoms either bond with three other atoms in a single-vacancy site or four atoms in a double-vacancy site in the graphene lattice, as can be directly observed from the images. Moreover, the enhanced signal-to-noise (S/N) ratio in the ADF images allows atom-by-atom chemical analysis via quantitative contrast analysis [20] at the Si defect sites. In both threefold and fourfold coordination cases, nitrogen atoms are sometimes found to replace one of the carbon atoms that bond directly with the Si impurities [Figs. 1(a) and 1(c)].

The ADF images provide the local chemical environment of the threefold and fourfold coordinated Si defect configurations, but do not reveal the nature or the three-dimensional configuration of the chemical bonds. Both configurations appear planar in the image, but they may not be. If they are indeed planar, threefold coordinated Si would have sp^2 bonding, whereas planar fourfold coordination would more likely have sp^2d hybridization [21], which has not been reported for Si so far. We address and

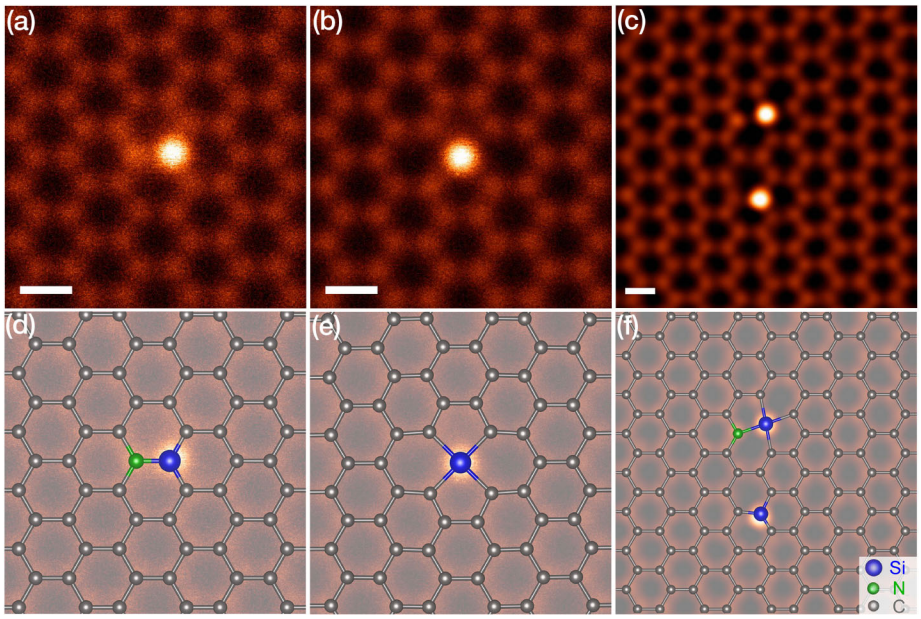

FIG. 1 (color online). Atomic structures for threefold and fourfold coordinated Si impurities in monolayer graphene. [(a)-(c)] STEM-ADF images of individual Si impurity atoms in the most common defect configurations with threefold or fourfold coordination. [(d)-(f)] Schematics of the structure models, overlaid with the corresponding ADF images, for the defect structures shown in (a)-(c), respectively. The chemical identity of each atom was obtained from quantitative ADF image analysis. Scale bars: 0.2 nm.

resolve these issues by analyzing the ELNES from various Si defects. Unlike the carbon atoms on a graphene edge that reconstruct under the electron beam [10,22], the substitutional Si impurities in the graphene lattice are stable under our optimized experimental conditions. This stability has been corroborated by DFT calculations [23]. The high structural stability ensures that no breaking or creation of bonds occurs during the spectrum imaging experiment, and the bonding information obtained from ELNES can be correlated with the local atomic configuration at the Si defects unambiguously.

Figure 2(a) shows two Si atoms in the graphene lattice, with different local atomic coordination, where STEM-EEL spectrum images [24,25] were acquired. The Si L edge ELNES spectra for the two Si defect configurations are shown in Fig. 2(b). The Si spectra were extracted from a 4×4 pixels^2 (i.e., 0.16×0.16 nm^2) region around each Si atom, and were acquired using a dwell time of 0.1 s per

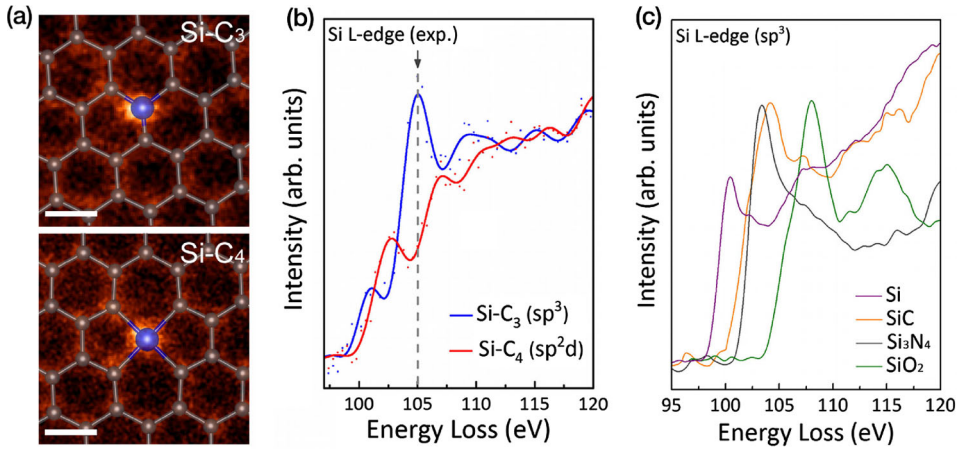

FIG. 2 (color online). ELNES for threefold and fourfold coordinated Si impurities in monolayer graphene. (a) ADF images and overlaid structure models for the threefold and fourfold coordinated Si impurity atoms in graphene, where EEL spectrum images were acquired. (b) Experimental ELNES for Si L edge from the threefold coordinated (blue or top) and fourfold coordinated (red or bottom) Si atoms shown in (a). The Si spectra were extracted from corresponding EEL spectrum images. (c) Reference Si L edge spectra from different bulk materials. Si in all these bulk materials adopts sp^3 hybridization, and each spectrum displays a sharp peak after the edge onset. The spectrum for SiC was digitized from Ref. [26]. Scale bars: 0.2 nm.

pixel and a probe current of about 100 pA, resulting in a total dose of $\sim 1.0 \times 10^9$ electrons per Si atom. The high electron dose setting used in the experiment unambiguously allows the identification of the fine structural features in the experimental spectra. The spectrum in blue (top) was taken from the threefold coordinated Si, bonded with three carbon atoms (denoted Si-C_3). The ELNES exhibits a sharp peak at 105 eV, right after the edge onset, followed by a steady increase above 107 eV. These features closely reproduce those recorded from bulk SiC [Figs. 2(c) and S1], where Si adopts sp^3 hybridization. The presence of a sharp peak right after the onset of the Si L edge is also characteristic in the ELNES from bulk Si, SiO_2, and Si_3N_4 [Fig. 2(c)], all with sp^3 hybridized Si. The similarity in ELNES, thus, suggests that Si in the Si-C_3 defect adopts the same sp^3 hybridization as that in SiC. In turn, the sp^3 hybridization features observed in the ELNES for the threefold coordinated Si allows us to further conclude that the configuration of the defect is not planar. Instead, the Si atom must be occupying a site above the plane of its three neighbors.

The red (bottom) spectrum in Fig. 2(b) was recorded from the fourfold coordinated Si, bonded with four carbon atoms (denoted Si-C_4). In contrast to the ELNES from Si-C_3, the sharp peak at 105 eV is absent for the fourfold coordinated Si, resulting in an almost-monotonic increase in excitation intensity after the onset of the Si L edge, with two small peaks at 102.6 and 107 eV. Moreover, the total Si L edge excitation intensity for the Si-C_4 structure is considerably lower than that from the Si in the threefold coordinated Si-C_3, due to the missing 105 eV peak [Fig. 2(b)].

Since the L edge spectra reflect the excitation of $2p$ electrons to unoccupied $3d$ states, the difference observed in the ELNES for the threefold and fourfold coordinated Si in graphene is a direct indication of different unoccupied density of $3d$ states due to different bonding configurations. The absence of a sharp peak after the onset of the Si L edge at 105 eV for the fourfold coordinated Si suggests a stronger mixing of the $3d$ states with the $3s$ and $3p$ states that make up the four Si-C bonds, forming sp^2d-like hybridization. Such hybridization allows us to further infer that this defect configuration is planar or nearly planar.

The above results, obtained solely through analysis of the experimental images and spectra have been confirmed by first-principles DFT calculations (see supplementary materials). First, the three-dimensional structures of the threefold and fourfold coordinated Si impurities in graphene were obtained. The fully relaxed structures are shown in Fig. 3(a). Consistent with previous theoretical reports [27,28], the Si atom displaces outwards from the graphene surface in the threefold coordinated case, while the fourfold coordinated Si atom stays practically in the same plane as the graphene lattice, in excellent agreement with the conclusions drawn from the experimental data.

We then calculated the ELNES of the Si L edge to correlate the experimental ELNES features with the nature of the chemical bonds at different atomic configurations of Si impurities. As shown in Figs. 3(b) and 3(c), the sharp peak at 105 eV and a weak shoulder at $\sim$101 eV for the threefold coordinated Si-C_3 defect were well reproduced by the calculations. The absence of the 105 eV sharp peak for the fourfold coordinated Si-C_4 defect was also confirmed by theory. The calculated spectra also reveal the presence of weaker peaks at 102.2 and 107 eV for the fourfold coordinated Si-C_4 defect, which were also observed at similar energy ranges in the experimental spectrum.

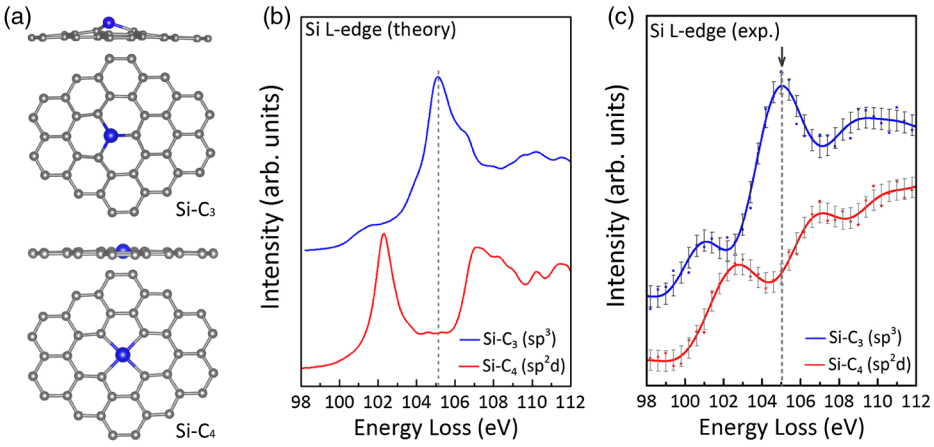

FIG. 3 (color online). Three-dimensional structure and ELNES for threefold and fourfold coordinated Si impurities in monolayer graphene. (a) Relaxed structures for the threefold and fourfold Si defect in a perfect graphene layer. Silicon: blue (top), carbon: gray. The Si atom in the threefold coordinated Si-C_3 structure is displaced $\sim$0.5 Å out of the graphene plane, while the Si atom in the fourfold Si-C_4 defect structure remains practically in the graphene plane. (b) Calculated Si L edge spectra for the threefold coordinated (blue or top) and fourfold coordinated (red or bottom) Si atoms in graphene. (c) Re-presentation of the experimental Si L edge spectra from the two different defect configurations shown in Fig. 2. The error bars were obtained by calculating the standard deviation of the background substracted spectra in the energy range of 85–98 eV.

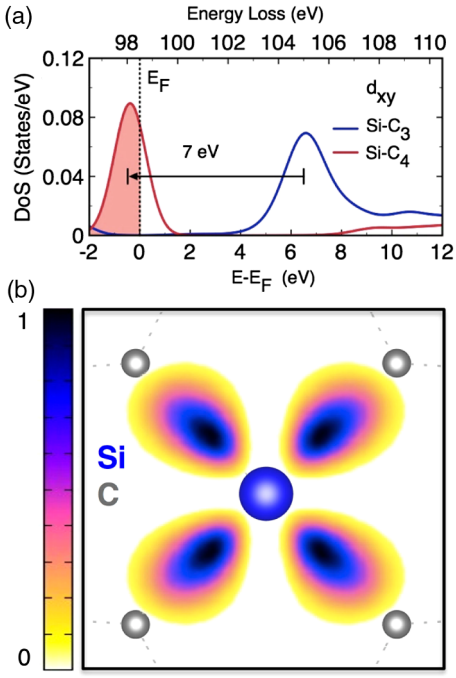

FIG. 4 (color online). Contribution of the Si $3d_{xy}$ orbital to the bonding of a fourfold coordinated Si atom in graphene. (a) pDOS of the Si d_{xy} orbital for the threefold and fourfold coordinated Si impurity atoms in the graphene lattice [as shown in Fig. 2(a)]. (b) Charge density distribution of the Si $3d_{xy}$ orbital around the fourfold coordinated Si-C_4 defect.

We further looked into the contribution from the different Si $3d$ orbitals to the partial density of states (pDOS) for the threefold and fourfold coordinated Si defects (see Supplemental Figs. S2–S5 for details). The sharp peak at 105 eV, observed for the threefold coordinated Si-C_3 defect, is mainly due to the $3d_{xy}$ and $d_{x^2-y^2}$ orbitals. Moreover, the $3d$ orbitals do not show significant density below the Fermi level (E_F), indicating that the bonding in the Si-C_3 case mainly involves the $3s$ and $3p$ electrons of Si. In contrast, a redistribution of the pDOS for the d_{xy} and $d_{x^2-y^2}$ orbitals is present for the fourfold coordinated Si in Si-C_4. Importantly, there is a considerable shift, about 7 eV, of the d_{xy} orbital's peak to lower energies, placing it below the Fermi level [Fig 4(a)], whereas the peak of the $d_{x^2-y^2}$ orbital is redistributed to higher energies. The redistribution of the density of empty Si d states in the Si-C_4 structure accounts for the disappearance of the peak at 105 eV for the Si L edge spectrum. Additionally, since the d_{xy} orbital is now below the Fermi level, i.e., occupied, it participates in the chemical bonding of the fourfold coordinated Si, and provides the desired spatial distribution of the charge density for the formation of four Si-C bonds in the xy plane.

The participation of the Si $3d_{xy}$ orbital in the chemical bonding for the planar Si-C_4 configuration is further confirmed by mapping out the charge distribution of the $3d_{xy}$ orbital around the Si defect, as shown in Fig. 4(b). The participation of the Si $3d_{xy}$ orbital in the chemical bond amounts to a sp^2d hybridization for Si, instead of the preferred sp^3 hybridization, as one can expect from Pauling's classical hybridization orbital theory [29] for planar fourfold coordinated structures. Therefore, the calculations confirm the inference that the absence of a sharp peak (at 105 eV in this case) after the Si L edge onset in the experimental ELNES for the fourfold coordinated Si defect [Fig. 3(c)] is a direct consequence and indication of the formation of sp^2d hybridization for Si.

In summary, we demonstrate that the bonding characteristics of individual impurities in two-dimensional materials can be revealed with a synergistic combination of aberration-corrected STEM-ADF imaging and STEM-EELS, with DFT calculations confirming and extending the conclusions. As two-dimensional materials become more prominent in nanoelectronic applications, the method presented here can potentially provide a valuable tool for their characterization. The work shown here also suggests that it would be possible in the near future to reveal the bonding characteristic of individual atoms in molecules and other low-dimensional materials using low-voltage aberration-corrected STEM.

This research was supported by National Science Foundation through Grant No. DMR-0938330 (W. Z.), Oak Ridge National Laboratory's Shared Research Equipment (ShaRE) User Program (J. C. I.), which is sponsored by the Office of Basic Energy Sciences, U.S. Department of Energy, the Materials Sciences and Engineering Division, Office of Basic Energy Sciences, U.S. Department of Energy (S. J. P., S. T. P.), and DOE Grant No. DE-FG02-09ER46554 (MDK, MPP, STP). This research used resources of the National Energy Research Scientific Computing Center, which is supported by the Office of Science of the U.S. Department of Energy under Contract No. DE-AC02-05CH11231. W. Z. and M. D. K. contributed equally to this work.

Note added in proof.—During the reviewing process it came to our attention that similar work was performed by Ramasse *et al.* at the SuperSTEM Laboratory in Daresbury, UK [30].

*To whom all correspondence should be addressed.
wu.zhou@vanderbilt.edu
idrobojc@ornl.gov
†Present address: Pacific Northwest National Laboratory, Richland, WA 99352, USA.

[1] J. A. Kubby and J. J. Boland, Surf. Sci. Rep. **26**, 61 (1996).
[2] L. Zhao *et al.*, Science **333**, 999 (2011).
[3] J. C. Meyer *et al.*, Nature Mater. **10**, 209 (2011).
[4] N. D. Browning, M. F. Chisholm, and S. J. Pennycook, Nature (London) **366**, 143 (1993).
[5] P. E. Batson, Nature (London) **366**, 727 (1993).

[6] D. A. Muller, Y. Tzou, R. Raj, and J. Silcox, Nature (London) **366**, 725 (1993).
[7] K. Suenaga, M. Tencé, C. Mory, C. Colliex, H. Kato, T. Okazaki, H. Shinohara, K. Hirahara, S. Bandow, and S. Iijima, Science **290**, 2280 (2000).
[8] M. Varela *et al.*, Phys. Rev. Lett. **92**, 095502 (2004).
[9] K. Suenaga *et al.*, Nature Chem. Biol. **1**, 415 (2009).
[10] K. Suenaga and M. Koshino, Nature (London) **468**, 1088 (2010).
[11] See Supplemental Material at http://link.aps.org/supplemental/10.1103/PhysRevLett.109.206803 for details of the STEM experiments and first-principles calculations.
[12] K. S. Kim, Y. Zhao, H. Jang, S. Y. Lee, J. M. Kim, K. S. Kim, J.-H. Ahn, P. Kim, J.-Y. Choi, and B. H. Hong, Nature (London) **457**, 706 (2009).
[13] Y. Lee, S. Bae, H. Jang, S. Jang, S.-E. Zhu, S. H. Sim, Y. I. Song, B. H. Hong, and J.-H. Ahn, Nano Lett. **10**, 490 (2010).
[14] C. Berger *et al.*, J. Phys. Chem. B **108**, 19912 (2004).
[15] K. V. Emtsev *et al.*, Nature Mater. **8**, 203 (2009).
[16] G. M. Rutter, J. N. Crain, N. P. Guisinger, T. Li, P. N. First, and J. A. Stroscio, Science **317**, 219 (2007).
[17] A. H. C. Neto, F. Guinea, N. M. R. Peres, K. S. Novoselov, and A. K. Geim, Rev. Mod. Phys. **81**, 109 (2009).
[18] T. Palacios, Nature Nanotech. **6**, 464 (2011).
[19] K. Kim, J.-Y. Choi, T. Kim, S.-H. Cho, H.-J. Chung, Nature (London) **479**, 338 (2011).
[20] O. L. Krivanek *et al.*, Nature (London) **464**, 571 (2010).
[21] W. Demtröder, *Atoms, Molecules and Photons. An Introduction to Atomic-, Molecular- and Quantum Physics* (Springer, Heidelberg, New York, 2011), 2nd ed.
[22] C. O. Girit *et al.*, Science **323**, 1705 (2009).
[23] W. Zhou, J. Lee, J. Nanda, S. T. Pantelides, S. J. Pennycook, and J.-C. Idrobo, Nature Nanotech. **7**, 161 (2012).
[24] C. Jeanguillaume and C. Colliex, Ultramicroscopy **28**, 252 (1989).
[25] J. A. Hunt and D. B. Williams, Ultramicroscopy **38**, 47 (1991).
[26] S. T. Pantelides *et al.*, *Proceeding of the International Conference on Silicon Carbide and Related Materials* (Research Triangle Park, North Carolina, 1999).
[27] P. A. Denis, Chem. Phys. Lett. **492**, 251 (2010).
[28] A. V. Krasheninnikov, P. O. Lehtinen, A. S. Foster, P. Pyykko, and R. M. Nieminen, Phys. Rev. Lett. **102**, 126807 (2009).
[29] L. Pauling, J. Am. Chem. Soc. **53**, 1367 (1931).
[30] Q. M. Ramasse, C. R. Seabourne, R. Zan, D. M. Kepaptsoglou, U. Bangert, and A. J. Scott (unpublished).